M-Al-*M* groups trapped in cages of $Al_{13}M_4$ (M=Co, Fe, Ni, Ru) complex intermetallic phases as seen via NMR

P. Jeglič,[1] S. Vrtnik,[1] M. Bobnar,[1] M. Klanjšek,[1] B. Bauer,[2] P. Gille,[2] Yu. Grin,[3] F. Haarmann,[4] and J. Dolinšek[1]

[1]*J. Stefan Institute, University of Ljubljana, Jamova 39, SI-1000 Ljubljana, Slovenia*

[2]*Department of Earth and Environmental Sciences, Crystallography Section, Ludwig-Maximilians-Universität München, Theresienstrasse 41, D-80333 München, Germany*

[3]*Max-Planck-Institut für Chemische Physik fester Stoffe, Nöthnitzer Str. 40, D-01187 Dresden, Germany*

[4]*Institut für Anorganische Chemie, RWTH Aachen, Landoltweg 1, D-52074 Aachen, Germany*

(Received 29 June 2010; published 3 September 2010)

The crystallographic structures of decagonal quasicrystals and their periodic approximants are traditionally described as a periodic stacking of atomic planes. By performing a ^{27}Al NMR spectroscopic study of the $Al_{13}M_4$ (M=transition metal) family of four-layer decagonal approximants, including the orthorhombic o-$Al_{13}Co_4$, the monoclinic $Al_{13}Fe_4$, its ternary derivative $Al_{13}(Fe,Ni)_4$, and the monoclinic $Al_{13}Ru_4$, we show that all these phases contain structural detail of a nearly linear *M*-Al-*M* atomic group trapped inside an elongated cage, resembling the three-dimensional (3D) "cage-compound" structure of the intermetallic clathrates. We determined the electric-field-gradient- (EFG) and the magnetic-shielding tensors at the Al site of the *M*-Al-*M* groups. The asymmetry parameter of the EFG tensor was estimated theoretically by a point-charge model, taking into account the charges of both the *M*-Al-*M* atoms and the surrounding cage atoms. The calculations support ionic bonding of the *M*-Al-*M* group to the cage atoms and the existence of a 3D chemical bonding network in the $Al_{13}M_4$ phases. The above results show that the traditional description of the $Al_{13}M_4$ decagonal approximant phases in terms of two-dimensional (2D) atomic layers stacked along the pseudotenfold crystallographic direction is a convenient geometrical approach to describe their complex structures but is not appropriate for the description of their physical properties, which should be analyzed by taking into account the full 3D nature of the chemical bonding framework. This favors the 3D cage-compound structural description of the $Al_{13}M_4$ phases over the pseudo-2D stacked-layer description.

DOI: 10.1103/PhysRevB.82.104201 PACS number(s): 61.44.Br, 76.60.−k

I. INTRODUCTION

The crystallographic structures of decagonal quasicrystals (*d*-QCs) and their periodic approximants are traditionally described as a periodic stacking of atomic planes with either quasiperiodic in-plane atomic order in the case of *d*-QCs or translationally periodic order in the case of the approximants.[1] Consequently, *d*-QCs are considered to be two-dimensional (2D) quasicrystals, whereas they are periodic crystals in the third dimension. Examples of the stacked-layer *d*-QC structures are *d*-Al-Ni-Co and *d*-Al-Cu-Co with two atomic layers within the periodicity length of about 0.4 nm along the stacking (tenfold) direction, *d*-Al-Co, *d*-Al-Ni, and *d*-Al-Si-Cu-Co with four layers within the periodicity length of about 0.8 nm, *d*-Al-Mn, *d*-Al-Cr, and *d*-Al-Mn-Pd with six layers within the periodicity length of about 1.2 nm and *d*-Al-Pd and *d*-Al-Cu-Fe with eight layers within the periodicity length of 1.6 nm. Decagonal approximant phases are characterized by large unit cells but preserve the stacked-layer structure with the periodicity lengths along the stacking direction almost identical to those of the *d*-QCs. The monoclinic $Al_{13-x}(Co_{1-y}Ni_y)_4$ decagonal approximant,[2] known as the *Y* phase of Al-Ni-Co, comprises two atomic layers within one periodic unit. The $Al_{13}M_4$ (M=transition metal) family with M=Co, Fe, Ru, Rh, Os represents four-layer approximant phases,[3–7] whereas the orthorhombic Al_4M phases, described by Deng *et al.*,[8] and the orthorhombic Taylor-phase[9,10] *T*-Al_3Mn represent six-layer approximant structures. However, recent analysis of the chemical bonding in the orthorhombic o-$Al_{13}Co_4$ four-layer approximant by means of the electron localizability indicator (ELI) (Refs. 11 and 12) has led to a highly unexpected result that has put the traditional view of the $Al_{13}M_4$ crystallographic structures in terms of the atomic layers under question. Numerous directed (covalent) Co-Al and Al-Al bonds were found within the atomic layers as well as in-between the layers, revealing the formation of a three-dimensional (3D) bonding framework, contrary to the traditional consideration in terms of 2D atomic layers. This has suggested that the stacked-layer description is a convenient geometrical approach to describe the complex structure of the o-$Al_{13}Co_4$ phase, whereas its physical properties are those of a true 3D solid. In addition, elongated cavities along the stacking direction were identified in the 3D framework with the nearly linear Co-Al-Co "guest" atomic groups trapped inside. The ELI analysis has shown that the interactions within the Co-Al-Co group atoms (directed, covalent) differ from those between this group and the atoms of the framework (nondirected, ionic). While the covalent bonding between the Co-Al-Co atoms is strong, bonding of the Co-Al-Co group to the rest of the lattice is weaker. This unusual feature reveals analogy to the intermetallic clathrates, which also exhibit covalently bonded 3D networks with filler atoms in the cavities, interacting ionically with the host framework. The ^{27}Al NMR spectroscopic study[13] of the o-$Al_{13}Co_4$ confirmed the results of the bonding analysis and supported the unique bonding situation of Al in the nearly linear Co-Al-Co groups.

In this paper, we report the ^{27}Al NMR study of the $Al_{13}M_4$ family of four-layer decagonal approximants, including the orthorhombic o-$Al_{13}Co_4$, the monoclinic $Al_{13}Fe_4$, its ternary derivative $Al_{13}(Fe,Ni)_4$, and the monoclinic $Al_{13}Ru_4$. By determining the electric-field-gradient- (EFG) and the magnetic-shielding tensors at the Al site of the *M*-Al-*M* groups, we show that the structural detail of nearly linear *M*-Al-*M* atomic groups (called the "*Würstchen*") trapped inside the elongated cages of the 3D network is present in all the above compounds. Consequently, the 3D bonding framework and the "cage-compound" structural description appear to be a common feature of the $Al_{13}M_4$ family.

II. SAMPLE SELECTION AND STRUCTURAL CONSIDERATIONS

A. o-$Al_{13}Co_4$

According to the original structural model of the o-$Al_{13}Co_4$ phase by Grin *et al.*,[3] the lattice parameters of the orthorhombic unit cell (space group $Pmn2_1$, Pearson symbol $oP102$) are $a=0.8158$ nm, $b=1.2342$ nm, and $c=1.4452$ nm with 102 atoms in the unit cell distributed over 10 Co and 28 Al crystallographic sites. Within the traditional stacked-layer description, the structure corresponds to a four-layer stacking along [100], with flat layers at $x=0$ and $x=1/2$ and two symmetrically equivalent puckered layers at $x=1/4$ and 3/4, giving ≈ 0.8 nm period along [100]. All lattice sites of the original model are fully occupied. Based on a recent more precise crystal structure determination, Grin *et al.*[12] have proposed a new model of the o-$Al_{13}Co_4$, where some sites of the original model are split, yielding partial occupation of the sites Al(14) and Al(25)-Al(32) (nine altogether) in the new model with the probabilities 0.715, 0.576, 0.516, 0.6, 0.351, 0.554, 0.192, 0.305, and 0.399, respectively.

The o-$Al_{13}Co_4$ single crystal used in our study was grown by the Czochralski technique and the growth details are described elsewhere.[14] Three bar-shaped specimens of dimensions $2\times2\times7$ mm^3 were cut from the parent crystal with their long edges along [100] (*a*), [010] (*b*), and [001] (*c*) crystallographic directions, where *a* is the pseudo tenfold direction of the o-$Al_{13}Co_4$ structure. Anisotropic physical properties of the o-$Al_{13}Co_4$ phase (the magnetic susceptibility, the electrical resistivity, the thermoelectric power, the Hall coefficient and the thermal conductivity), measured on the same set of samples, were reported recently.[15]

B. $Al_{13}Fe_4$ and $Al_{13}(Fe,Ni)_4$

According to the original structural model of $Al_{13}Fe_4$ by Grin *et al.*,[4] lattice parameters of the monoclinic unit cell (space group $C2/m$, Pearson symbol $mC102$) are $a=1.5492$ nm, $b=0.8078$ nm, $c=1.2471$ nm, and $\beta=107.69°$ with 102 atoms in the unit cell distributed over five Fe and 15 Al crystallographic sites. All lattice sites are fully occupied except the site Al(2) that shows partial occupation of 0.92 ± 0.02. The structure can be described as a four-layer stacking along [010] with flat layers at $y=0$ and $y=1/2$ and two symmetrically equivalent puckered layers at $y=1/4$ and 3/4, giving ≈ 0.8 nm period along [010]. Based on a recent high-resolution x-ray diffraction study, the structural model of $Al_{13}Fe_4$ has been refined.[17] The atomic coordinates of the refined model are within three estimated standard deviation (e.s.d.) equal to the atomic coordinates of the original model, whereas the occupancy of the position Al(15) (that corresponds to the partially occupied position Al(2) of the original model) was found to be 1 within one e.s.d., so that all lattice sites of the refined model are fully occupied. Thus, in comparison with many other members of the $Al_{13}M_4$ family, the $Al_{13}Fe_4$ reveals a nearly completely ordered crystal structure.

The $Al_{13}(Fe,Ni)_4$ phase is a ternary solid solution of Ni in $Al_{13}Fe_4$ with the maximum solubility of Ni 8.9 at. %.[16] The chemical composition of the $Al_{13}(Fe,Ni)_4$ single crystal used in our investigations was $Al_{76.5}Fe_{21.3}Ni_{2.2}$. The introduction of a small amount of Ni atoms into the structure of the ternary extension $Al_{13}(Fe,Ni)_4$ (about 2 at. % in our case) creates positional and substitutional disorder within the more or less perfect $Al_{13}Fe_4$ structure so that the $Al_{13}(Fe,Ni)_4$ can be viewed as a disordered variant of the structurally well ordered $Al_{13}Fe_4$.

The $Al_{13}Fe_4$ and $Al_{13}(Fe,Ni)_4$ single crystals used in our study were grown by the Czochralski technique and the details of preparation are described elsewhere.[14] Three bar-shaped samples of dimensions $1\times1\times8$ mm^3 were prepared for each compound with their long edges along three orthogonal directions. The long edge of the first sample was along the [010] stacking direction (designated in the following as *b*), which corresponds to the periodic tenfold direction in the related *d*-QCs. The (*a*,*c*) monoclinic plane corresponds to the quasiperiodic plane in the *d*-QCs and the second sample was cut with its long edge along the [001] (*c*) direction, whereas the third one was cut along the direction perpendicular to the (*b*,*c*) plane. This direction is designated as a^* (it lies in the monoclinic plane at an angle 17.69° with respect to *a* and perpendicular to *c*). The anisotropic physical properties of the $Al_{13}Fe_4$ and $Al_{13}(Fe,Ni)_4$ samples used in our study (the magnetic susceptibility, the electrical resistivity, the thermoelectric power, the Hall coefficient, and the thermal conductivity) were determined recently.[17]

C. $Al_{13}Ru_4$

The $Al_{13}Ru_4$ monoclinic phase is isostructural to $Al_{13}Fe_4$. Our $Al_{13}Ru_4$ oriented single crystal was grown by the Czochralski technique following similar steps as in the case of the $Al_{13}Fe_4$. In the NMR experiments, the oriented crystal was rotated around the a^*, *b*, and *c* crystallographic directions. Magnetic characterization of the sample (not shown) has revealed that the $Al_{13}Ru_4$ is diamagnetic, in contrast to the o-$Al_{13}Co_4$, $Al_{13}Fe_4$, and $Al_{13}(Fe,Ni)_4$, which are weak paramagnets.

III. NMR DETERMINATION OF THE EFG AND THE MAGNETIC SHIELDING TENSORS

The EFG- and the magnetic-shielding tensors were determined from the rotation patterns of the ^{27}Al (spin I=5/2) central transition ($1/2\rightarrow-1/2$) NMR spectra. The ^{27}Al nu-

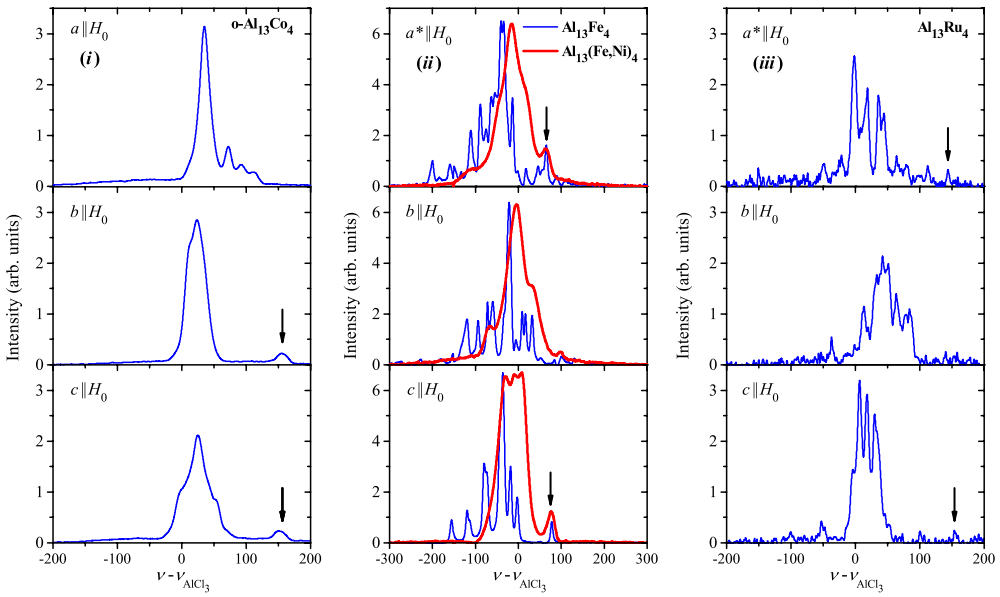

FIG. 1. (Color online) Panel (i): ^{27}Al central-transition NMR spectra of the single-crystalline o-$Al_{13}Co_4$ for the magnetic field oriented along the a, b, and c crystallographic directions. The line corresponding to the Al site of the Co-Al-Co group is shown by an arrow in the $b\|H_0$ and $c\|H_0$ spectra. Panel (ii): ^{27}Al central-line NMR spectra of the single-crystalline $Al_{13}Fe_4$ and $Al_{13}(Fe,Ni)_4$ for the magnetic field oriented along the a^*, b, and c crystallographic directions. The lines corresponding to the Al site of the M-Al-M groups are shown by arrows in the $a^*\|H_0$ and $c\|H_0$ spectra. Panel (iii): ^{27}Al central-line NMR spectra of the single-crystalline $Al_{13}Ru_4$ for the magnetic field oriented along the a^*, b, and c crystallographic directions. The line corresponding to the Al site of the Ru-Al-Ru group is shown by an arrow in the $a^*\|H_0$ and $c\|H_0$ spectra.

clei interact with the surrounding ions and electrons by the electrical and magnetic interactions and the number of absorption lines in a given $m\rightarrow m-1$ spin transition equals the number of magnetically inequivalent ^{27}Al crystallographic sites within the unit cell. The central-transition NMR frequency ν_i of the ith ^{27}Al crystallographic site in a magnetic field H_0 can be written as a sum[18]

$$\nu_i - \nu_0 = \nu_{quad,i}^{(2)} + \nu_{mag,i}, \tag{1}$$

where $\nu_0=\gamma_n H_0/2\pi$ is the Zeeman frequency and γ_n is the nuclear gyromagnetic ratio. The term $\nu_{quad,i}^{(2)}$ is the second-order electric quadrupole shift

$$\nu_{quad,i}^{(2)} = \frac{\nu_{Q,i}^2}{12\nu_0}\{6\sin^2\theta_i(1-9\cos^2\theta_i) - 4\eta_i\cos 2\phi_i\sin^2\theta_i(9\cos^2\theta_i+1) + \eta_i^2 \times(-16/3+8\cos^2\theta_i+6\cos^2 2\phi_i\sin^4\theta_i)\}. \tag{2}$$

The quadrupole coupling constant $\nu_{Q,i}=\frac{3eQV_{ZZ}^{(i)}}{20h}$ is determined by the largest principal value $V_{ZZ}^{(i)}$ of the EFG tensor at the lattice site i, which can be written as[18]

$$V_{ZZ}^{(i)} = V_{ZZ,i}^{ion}(1-\gamma_\infty^{(i)}) + V_{ZZ,i}^{el}. \tag{3}$$

The first term on the right of Eq. (3) originates from the neighboring ionic charges, enhanced by the Sternheimer antishielding factor $1-\gamma_\infty^{(i)}$ due to the ionic electric field polarization of the core electrons whereas the second term originates from the charges of the electrons. The angles θ_i and ϕ_i in Eq. (2) describe the orientation of the applied magnetic field with respect to the principal-axes system (PAS) of the EFG tensor, and $\eta_i=(V_{XX}^{(i)}-V_{YY}^{(i)})/V_{ZZ}^{(i)}$ is the quadrupole asymmetry parameter, where $|V_{XX}^{(i)}|\leq|V_{YY}^{(i)}|\leq|V_{ZZ}^{(i)}|$.

The term $\nu_{mag,i}$ in Eq. (1) represents the frequency shift due to the coupling of the nuclear spin I with the magnetic field H_0 via the magnetic-shielding tensor S_{ij}, originating from the electronic surrounding. Generally, the magnetic-shielding tensor contains the chemical shift tensor σ_{ij} due to the electrons in the molecular orbitals and the Knight shift tensor K_{ij} due to the conduction electrons.[19] The frequency shift due to the magnetic-shielding tensor can be written as

$$\nu_{mag,i} = \frac{\gamma_n}{2\pi}\left[S_{iso}^{(i)} + \frac{S_{ZZ}^{(i)}}{2}(3\cos^2\theta_i' - 1 + \varepsilon_i\sin^2\theta_i'\cos 2\phi_i')\right]H_0. \tag{4}$$

Here $S_{iso}^{(i)}$ is the isotropic magnetic shift (the sum of the isotropic chemical shift $\sigma_{iso}=(1/3)\mathrm{Tr}\{\sigma_{ij}\}$ and the isotropic Knight shift K_{iso} due to the contact interaction between the nucleus and the s-type conduction electrons) whereas the parameters $S_{ZZ}^{(i)}$ and $\varepsilon_i=\frac{S_{XX}^{(i)}-S_{YY}^{(i)}}{S_{ZZ}^{(i)}}$ are the largest principal value and the asymmetry parameter of the traceless anisotropic magnetic-shielding tensor. The angles θ_i' and ϕ_i' describe the orientation of the magnetic field with respect to the PAS of the magnetic-shielding tensor.

Our ^{27}Al central-line NMR rotation patterns were performed at the temperature $T=80$ K in the magnetic field of 9.39 T. The origin of the frequency scale was taken at the resonance frequency of the $AlCl_3$ aqueous solution, $\nu_{AlCl_3}=104.223$ MHz.

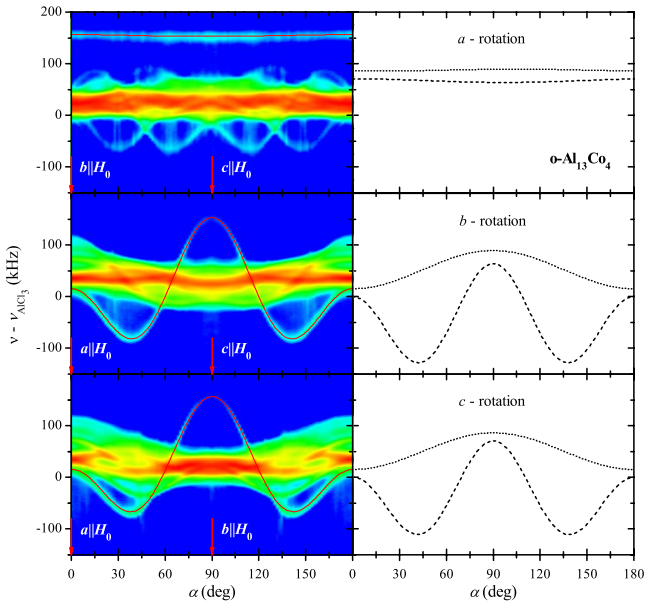

FIG. 2. (Color online) Rotation patterns of the ^{27}Al central-line spectra of o-$Al_{13}Co_4$ around the a, b, and c axes of the orthorhombic unit cell. The left column shows the experimental rotation patterns. Solid curves (red online) are the theoretical rotation patterns for the Al site of the Co-Al-Co groups, calculated from Eqs. (1)–(4). In the right column, the theoretical rotation patterns are decomposed into the EFG- (dashed curves) and the magnetic-shielding (dotted curves) contributions and are shown side by side to the experimental ones.

A. o-$Al_{13}Co_4$

Representative ^{27}Al central-line spectra of the o-$Al_{13}Co_4$ for the orientations $a\|H_0$, $b\|H_0$, and $c\|H_0$ are displayed in Fig. 1, panel (i). Most of the ^{27}Al lines from the 28 Al crystallographic sites in the unit cell overlap and are located roughly within the frequency interval $\nu-\nu_{AlCl_3}\in(-50,100$ kHz). There exists, however, one particular line with a stronger shift that is marked by an arrow in the $b\|H_0$ and $c\|H_0$ spectra at the frequency $\nu-\nu_{AlCl_3}\approx 160$ kHz. The experimental rotation patterns around the a, b, and c axes of the orthorhombic unit cell are shown in Fig. 2 (left column). It is observed that the above-mentioned line exhibits a particularly strong orientation dependence for the rotations about the b and c axes, whereas for the a rotation, its position at $\nu-\nu_{AlCl_3}\approx 160$ kHz is almost orientation independent. The strong frequency shift of this line indicates that the EFG and/or the magnetic shielding at the corresponding ^{27}Al site are considerably larger than at other ^{27}Al sites of the unit cell. Considering the EFG, its tensor elements depend on the distance r between the ^{27}Al resonant nucleus and the neighboring electric charges as $1/r^3$ so that the charges around this site should be closer to the ^{27}Al nucleus than at any other Al site. Moreover, the almost orientation-independent position of this line for the a rotation reveals that both the EFG- and the magnetic-shielding tensors are almost axially symmetric around the a crystallographic axis. Since this particular ^{27}Al line is well resolved from the rest of the ^{27}Al intensity in the NMR rotation patterns, we are able to determine its EFG- and magnetic-shielding tensors, whereas the overlapping intensity of the rest of the Al sites prevents the determination of their corresponding tensors.

The EFG- and the magnetic-shielding tensors were determined in the crystal-fixed (a,b,c) orthogonal reference frame by using Eqs. (1)–(4). The theoretical rotation patterns are shown by solid curves over the experimental data in the left column of Fig. 2. The resulting EFG tensor V_{ij} and its asymmetry parameter η, the anisotropic magnetic-shielding tensor S_{ij} and its asymmetry parameter ε, the isotropic magnetic shift S_{iso} and the quadrupole coupling constant ν_Q are given in Table I. The theoretical rotation patterns, decomposed into the EFG- and the magnetic-shielding contributions, are shown in Fig. 2 (right column) side by side to the experimental ones. For both tensors, the largest (absolute) principal value points along the a axis (V_{aa} and S_{aa}) of the orthorhombic unit cell, whereas the off-diagonal elements V_{ab}, V_{ac} and S_{ab}, S_{ac} are zero, indicating that the tensors are invariant to the $a\rightarrow -a$ transformation (i.e., the corresponding ^{27}Al site should be located either on the (100) mirror plane or on a twofold axis along [100]). The asymmetry

TABLE I. The EFG tensors ($\boldsymbol{V}$) and their asymmetry parameters η, the quadrupole coupling constants ν_Q, the anisotropic magnetic-shielding tensors $\boldsymbol{S}$ and their asymmetry parameters ε, and the isotropic magnetic shifts S_{iso} of the investigated $Al_{13}M_4$ phases.

	o-$Al_{13}Co_4$	$Al_{13}Fe_4$	$Al_{13}(Fe,Ni)_4$	$Al_{13}Ru_4$
$\boldsymbol{V}$ (10^{21} V/m^2)	$\begin{bmatrix} 7.03 & 0 & 0 \\ 0 & -3.77 & 0.06 \\ 0 & 0.06 & -3.26 \end{bmatrix}$	$\begin{bmatrix} 3.03 & 0 & 0.08 \\ 0 & -6.81 & 0 \\ 0.08 & 0 & 3.78 \end{bmatrix}$	$\begin{bmatrix} 3.07 & 0 & 0.31 \\ 0 & -6.77 & 0 \\ 0.31 & 0 & 3.70 \end{bmatrix}$	$\begin{bmatrix} 3.65 & 0 & -0.23 \\ 0 & -8.16 & 0 \\ -0.23 & 0 & 4.51 \end{bmatrix}$
η	0.07	0.11	0.13	0.12
ν_Q (MHz)	3.74	3.62	3.60	4.34
S (ppm)	$\begin{bmatrix} -463 & 0 & 0 \\ 0 & 217 & 8 \\ 0 & 8 & 246 \end{bmatrix}$	$\begin{bmatrix} 246 & 0 & 46 \\ 0 & -519 & 0 \\ 46 & 0 & 273 \end{bmatrix}$	$\begin{bmatrix} 226 & 0 & 19 \\ 0 & -491 & 0 \\ 19 & 0 & 265 \end{bmatrix}$	$\begin{bmatrix} 285 & 0 & -8 \\ 0 & -575 & 0 \\ -8 & 0 & 290 \end{bmatrix}$
S_{iso} (ppm)	609	−175	−140	278
ε	0.07	0.18	0.11	0.03

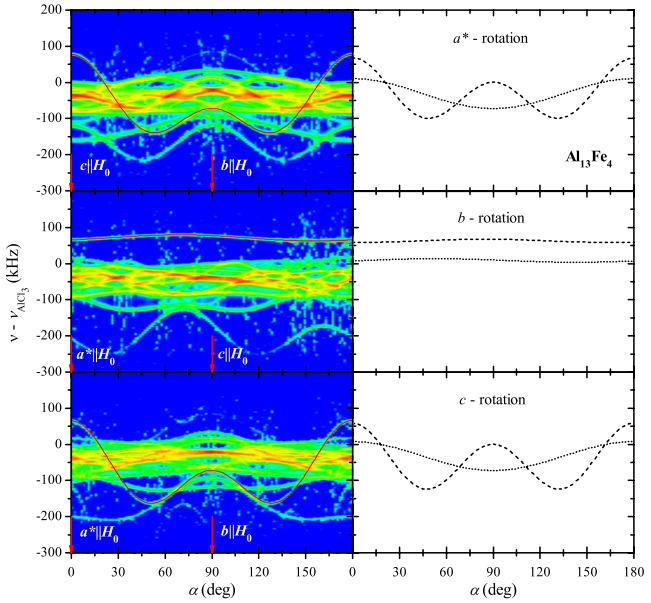

FIG. 3. (Color online) Rotation patterns of the ^{27}Al central-line spectra of $Al_{13}Fe_4$ around the a^*, b, and c orthogonal axes. The left column shows the experimental rotation patterns. Solid curves (red online) are the theoretical rotation patterns for the Al site of the Fe-Al-Fe group, calculated from Eqs. (1)–(4). In the right column, the theoretical rotation patterns are decomposed into the EFG- (dashed curves) and the magnetic-shielding (dotted curves) contributions and are shown side by side to the experimental ones.

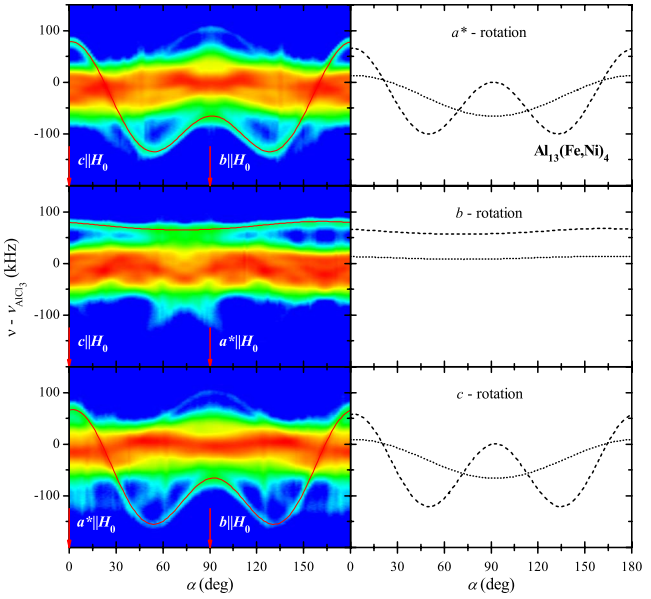

FIG. 4. (Color online) Rotation patterns of the ^{27}Al central-line spectra of $Al_{13}(Fe,Ni)_4$ around the a^*, b, and c orthogonal axes. The left column shows the experimental rotation patterns. Solid curves (red online) are the theoretical rotation patterns for the Al site of the M-Al-M group, calculated from Eqs. (1)–(4). In the right column, the theoretical rotation patterns are decomposed into the EFG- (dashed curves) and the magnetic-shielding (dotted curves) contributions and are shown side by side to the experimental ones.

parameters of both tensors (obtained after the tensors' diagonalization) are small, $\eta=0.07$ and $\varepsilon=0.07$ (with the uncertainty ± 0.02), demonstrating that the tensors are almost axially symmetric around the a axis. The above results are compatible with the structural detail of nearly linear Co-Al-Co atomic groups within a chemical environment of approximate axial symmetry along [100]. In that case, the closest charges to the Al nucleus would originate from the electronic density localized on the Al-Co covalent bonds of the Co-Al-Co group.

B. $Al_{13}Fe_4$ and $Al_{13}(Fe,Ni)_4$

The ^{27}Al central-line spectra of the monoclinic $Al_{13}Fe_4$ and $Al_{13}(Fe,Ni)_4$ at $T=80$ K for the orientations $a^*\|H_0$, $b\|H_0$, and $c\|H_0$ are displayed superimposed in Fig. 1, panel (ii). We observe that for all three orientations, the spectrum of the $Al_{13}Fe_4$ is a multiplet of sharp lines, originating from 15 different Al crystallographic sites in the monoclinic unit cell, whereas the spectrum of the $Al_{13}(Fe,Ni)_4$ is broad and more or less featureless, extending over the entire frequency range of the $Al_{13}Fe_4$ spectrum. This broadening can be explained by the positional and substitutional disorder in the $Al_{13}(Fe,Ni)_4$ lattice, created by the introduction of about 2 at. % of Ni. Due to the random disorder, the local chemical environment of a given Al crystallographic site no more repeats exactly over the subsequent unit cells, so that the resonance frequency becomes smeared, the individual lines in the spectrum become inhomogeneously broadened and the structure of sharp lines of a perfect lattice is replaced by a more or less featureless single broad line of a disordered lattice. This is indeed observed in Fig. 1, panel (ii), where the broad spectrum of the $Al_{13}(Fe,Ni)_4$ replaces the sharp structure of the $Al_{13}Fe_4$ spectrum, confirming that the $Al_{13}(Fe,Ni)_4$ can be viewed as a disordered version of the structurally well ordered $Al_{13}Fe_4$.

The experimental rotation patterns around the a^*, b, and c orthogonal axes are shown in Fig. 3 (left column) for the $Al_{13}Fe_4$ and in Fig. 4 (left column) for the $Al_{13}(Fe,Ni)_4$. The line with a particularly strong orientation-dependent shift for the a^* and c rotations and an almost orientation-independent shift for the b rotation, analogous to the one assigned to the Co-Al-Co aluminum site of the o-$Al_{13}Co_4$, is observed also for the $Al_{13}Fe_4$ and $Al_{13}(Fe,Ni)_4$. This line is marked by an arrow in the $a^*\|H_0$ and $c\|H_0$ spectra of Fig. 1, panel (ii) at the frequency $\nu-\nu_{AlCl_3}\approx 80$ kHz.

The EFG- and the magnetic-shielding tensors were determined in the crystal-fixed (a^*,b,c) orthogonal reference frame. The theoretical rotation patterns are shown by solid curves over the experimental data in the left column of Figs. 3 and 4. The V_{ij}, η, S_{ij}, ε, S_{iso}, and ν_Q parameters of the $Al_{13}Fe_4$ and $Al_{13}(Fe,Ni)_4$ are given in Table I. The theoretical rotation patterns, decomposed into the EFG- and the magnetic-shielding contributions, are shown in the right column of Figs. 3 and 4 side by side to the experimental ones. For both compounds, the largest (absolute) principal value of the EFG and the magnetic-shielding tensor points along the b axis (V_{bb} and S_{bb}) of the monoclinic unit cell whereas the off-diagonal elements V_{a^*b}, V_{bc} and S_{a^*b}, S_{bc} are zero, indicating that the tensors are invariant to the $b\rightarrow -b$ transfor-

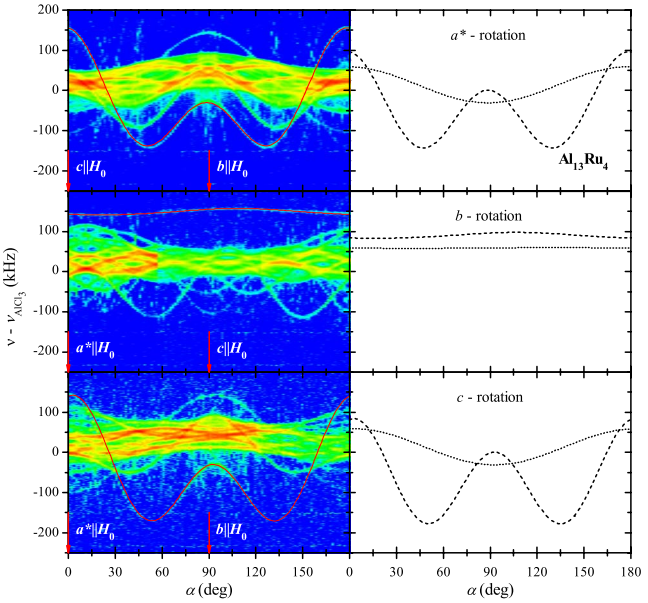

FIG. 5. (Color online) Rotation patterns of the ^{27}Al central-line spectra of $Al_{13}Ru_4$ around the a^*, b, and c orthogonal axes. The left column shows the experimental rotation patterns. Solid curves (red online) are the theoretical rotation patterns for the Al site of the Ru-Al-Ru group, calculated from Eqs. (1)–(4). In the right column, the theoretical rotation patterns are decomposed into the EFG- (dashed curves) and the magnetic-shielding (dotted curves) contributions and are shown side by side to the experimental ones.

mation (i.e., the corresponding ^{27}Al site should be located either on the (010) mirror plane or on a twofold axis along [010]). The asymmetry parameters of the tensors are small for both compounds, amounting $\eta=0.11$ and $\varepsilon=0.18$ for the $Al_{13}Fe_4$ whereas $\eta=0.13$ and $\varepsilon=0.11$ for the $Al_{13}(Fe,Ni)_4$. This again demonstrates that the tensors are almost axially symmetric around the b axis, a result that is compatible with the structural detail of nearly linear M-Al-M atomic groups (with M=Fe,Ni) in an approximately axially symmetric chemical environment along [010].

C. $Al_{13}Ru_4$

The ^{27}Al NMR spectrum of the monoclinic $Al_{13}Ru_4$ is analogous to that of the $Al_{13}Fe_4$. The ^{27}Al central-line spectra of the $Al_{13}Ru_4$ at $T=80$ K for the orientations $a^*\|H_0$, $b\|H_0$, and $c\|H_0$ are displayed in Fig. 1, panel (iii). The spectra consist of a multiplet of sharp lines, showing that the $Al_{13}Ru_4$ crystal is structurally well ordered. The experimental rotation patterns around the a^*, b, and c orthogonal axes are shown in Fig. 5 (left column). The line with a particularly strong orientation-dependent shift for the a^* and c rotations and an almost orientation-independent shift for the b rotation is observed also for the $Al_{13}Ru_4$. This line is marked by an arrow in the $a^*\|H_0$ and $c\|H_0$ spectra of Fig. 1, panel (iii) at the frequency $\nu-\nu_{AlCl_3}\approx 150$ kHz.

The EFG- and the magnetic-shielding tensors were determined in the crystal-fixed (a^*,b,c) orthogonal reference frame. The theoretical rotation patterns are shown by solid curves over the experimental data in the left column of Fig. 5. The resulting V_{ij}, η, S_{ij}, ε, S_{iso}, and ν_Q parameters are given in Table I. The theoretical rotation patterns, decomposed into the EFG- and the magnetic-shielding contributions, are shown in the right column of Fig. 5 side by side to the experimental ones. The largest (absolute) principal value of the EFG and the magnetic-shielding tensor points along the b axis (V_{bb} and S_{bb}) of the monoclinic unit cell, whereas the off-diagonal elements V_{a^*b}, V_{bc} and S_{a^*b}, S_{bc} are zero, indicating that the corresponding ^{27}Al site should be located either on the (010) mirror plane or on a twofold axis along [010]. The asymmetry parameter of the EFG tensor is small, amounting $\eta=0.12$, whereas the asymmetry parameter of the magnetic-shielding tensor is almost zero, $\varepsilon=0.03$, demonstrating an approximate axial symmetry around the b axis. The structural detail of a nearly linear Ru-Al-Ru atomic group in a chemical environment of approximate axial symmetry along [010] thus applies to the $Al_{13}Ru_4$ as well.

IV. DISCUSSION

A. Structural analysis

The nearly linear M-Al-M atomic groups can be easily identified within the existing structural models of the $Al_{13}M_4$ phases. In the following we perform the analysis for the original[3] and the new[12] structural model of the orthorhombic o-$Al_{13}Co_4$ and for the original[4] and the refined[17] model of the monoclinic $Al_{13}Fe_4$. The $Al_{13}(Fe,Ni)_4$ is a disordered version of the $Al_{13}Fe_4$ whereas the $Al_{13}Ru_4$ is isomorphic to the $Al_{13}Fe_4$ so that the same analysis applies to these two compounds as well. The two o-$Al_{13}Co_4$ models both contain two slightly different Co-Al-Co groups, four altogether in the unit cell. Within the original o-$Al_{13}Co_4$ model,[3] these are the Co(9)-Al(17)-Co(9) group with the Co-Al-Co angle $\beta=170.46°$ and the Co(10)-Al(28)-Co(10) group with the angle $\beta=168.30°$. Within the new o-$Al_{13}Co_4$ model[12] (where the atoms are numbered differently), these atomic groups are slightly more straight (closer to linearity). The angle of the Co(9)-Al(23)-Co(9) group is $\beta=175.14°$, whereas that of the Co(10)-Al(24)-Co(10) amounts 174.66°. The above structural parameters, including the Co-Al distances, are collected in Table II. In the structural models of the $Al_{13}Fe_4$, there exists only one type of an Fe-Al-Fe group, but again four in the unit cell. Within the original $Al_{13}Fe_4$ model,[4] this is the Fe(5)-Al(2)-Fe(5) group with the Fe-Al-Fe angle $\beta=176.87°$, whereas in the refined model,[17] this is the Fe(5)-Al(15)-Fe(5) group that is again slightly closer to linearity, with the Fe-Al-Fe angle amounting 177.18°. The structural parameters, including the Fe-Al distances, are also collected in Table II. The Fe-Al-Fe groups within the unit cell of the refined $Al_{13}Fe_4$ model are shown in Fig. 6(a).

The nearly axially symmetric atomic coordination around the M-Al-M groups can also be visualized from the existing $Al_{13}M_4$ structural models. The first coordination shell forms an elongated cage composed of Al atoms. In Fig. 6(a), a cage composed of 16 Al atoms around one of the Fe-Al-Fe groups is shown for the refined $Al_{13}Fe_4$ model. In Figs. 6(b) and 6(c), a cage around the Co(10)-Al(24)-Co(10) group is shown using the new structural model of the o-$Al_{13}Co_4$ phase. The atomic sites of the cage are arranged into two

TABLE II. Identification of the nearly linear *M*-Al-*M* atomic groups, the *M*-Al distances, the *M*-Al-*M* angles β and the *M* and Al crystallographic sites from the analysis of the existing structural models of the o-$Al_{13}Co_4$ and $Al_{13}Fe_4$ phases.

Model	*M*-Al-*M* group	*M*-Al distance (Å)	β (deg)	Al site	*M* site
o-$Al_{13}Co_4$ [new (Ref. 12)]	Co(9)-Al(23)-Co(9)	2.2451	175.14	$2a,m..$	$4b,1$
	Co(10)-Al(24)-Co(10)	2.2808	174.66	$2a,m..$	$4b,1$
o-$Al_{13}Co_4$ [original (Ref. 3)]	Co(9)-Al(17)-Co(9)	2.2455	170.46	$2a,m..$	$4b,1$
	Co(10)-Al(28)-Co(10)	2.3118	168.30	$2a,m..$	$4b,1$
$Al_{13}Fe_4$ [refined (Ref. 17)]	Fe(5)-Al(15)-Fe(5)	2.3735	177.18	$4i,m$	$8j,1$
$Al_{13}Fe_4$ [original (Ref. 4)]	Fe(5)-Al(2)-Fe(5)	2.3742	176.87	$4i,m$	$8j,1$

inner pentagonal rings and two outer triangles at both end caps, giving fairly axially symmetric atomic arrangement along the *M*-Al-*M* direction. However, the end triangles are not equilateral but isosceles so that the exact axial symmetry of the cage is broken and can be considered as a pseudoaxial symmetry only. This is evident from Figs. 6(b) and 6(c), where a cage with its Co-Al-Co guest is shown from two perspectives: the panel (b) shows the view along the [100] direction, where the isosceles top triangle is clearly evident, whereas the panel (c) shows the view from the perpendicular direction. The important result of the above structural analysis is the fact that the structures of the $Al_{13}M_4$ phases contain the detail of a nearly linear *M*-Al-*M* atomic group embedded in an elongated cage of approximate but not exact axial symmetry. For the cage of the new o-$Al_{13}Co_4$ model shown in Figs. 6(b) and 6(c), another departure from axial symmetry follows from the fact that some atomic sites of the cage are partially occupied because of a too close distance between the sites. Such a situation appears in the end-cap isosceles triangle of the cage shown in Fig. 6(b), where the distance between the atomic sites Al(29) and Al(31) amounts about 1.7 Å. This is too short for both sites to be populated simultaneously so that one of the atoms is absent in a real cage and the departure from the axial symmetry of the cage is further increased. In the refined $Al_{13}Fe_4$ model, all lattice sites are fully occupied (the end-cap triangle is closer to equilateral) so that this problem is not present.

We also note that the two crystallographically different Co-Al-Co groups together with their surrounding cages within the o-$Al_{13}Co_4$ orthorhombic unit cell are so similar to each other that we could not distinguish them from the ^{27}Al NMR spectra. For that reason, the single EFG- and the magnetic-shielding tensors determined for the o-$Al_{13}Co_4$ phase should be considered valid for both types of the Co-Al-Co groups (or to represent an average over the two group types).

B. EFG tensor symmetry analysis

The structural detail of a linearlike *M*-Al-*M* atomic group trapped inside an elongated cage of a pseudoaxial symmetry can also be inferred from the symmetry analysis of the EFG- and the magnetic-shielding tensors presented in Table I. A theoretical simulation of the magnetic-shielding tensor requires knowledge of the molecular orbitals of the *M*-Al-*M* group (to derive the chemical shift tensor) and the wave functions of the conduction electrons (for the Knight shift tensor), which are not known in our cases. The simulation of the EFG tensor is more straightforward, by adopting the point-charge approximation. In the following, we present a point-charge simulation of the EFG tensor at the Al position of the *M*-Al-*M* group by using the structural data of the original and the new models of the o-$Al_{13}Co_4$ and the original and the refined models of the $Al_{13}Fe_4$. We calculate the

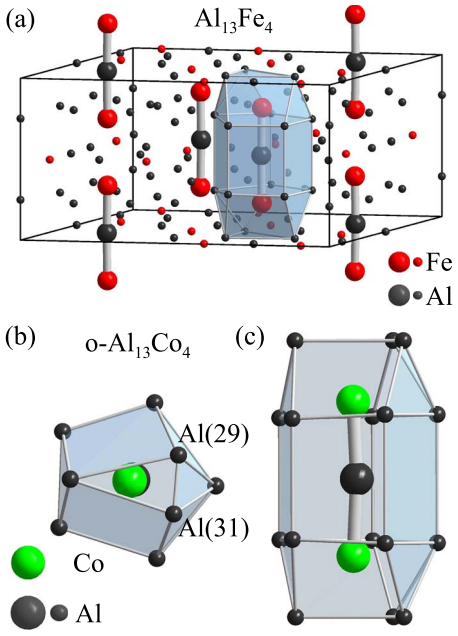

FIG. 6. (Color online) (a) The four linearlike Fe-Al-Fe groups within the monoclinic unit cell of the refined $Al_{13}Fe_4$ model (Ref. 17). The groups extend along the [010] direction. The Al atoms are shown by black circles and the Fe atoms by gray (red online) circles. A cage composed of 16 Al atoms around one of the Fe-Al-Fe groups is also shown. (b) The structural detail of a Co(10)-Al(24)-Co(10) group trapped inside a cage composed of Al atoms for the new structural model of the o-$Al_{13}Co_4$ phase (Ref. 12) (top view along the [100] direction). The Al atoms are shown by black circles and the Co atoms by gray (green online) circles. The partially occupied sites Al(29) and Al(31) at the end-cap isosceles triangle are marked. In panel (c), the same cage is shown from the perpendicular direction.

theoretical value of the EFG-tensor asymmetry parameter η by considering (i) only the charges on the M-Al-M group and (ii) also the charges of the surrounding cage (for the new o-$Al_{13}Co_4$ and the refined $Al_{13}Fe_4$ models only) and compare the theoretical η values to the experimental ones given in Table I.

The symmetry of the experimentally determined EFG tensors, where two out of three off-diagonal elements are zero [$V_{ab}=V_{ac}=0$ for the o-$Al_{13}Co_4$ and $V_{a^*b}=V_{bc}=0$ for the $Al_{13}Fe_4$, $Al_{13}(Fe,Ni)_4$ and $Al_{13}Ru_4$], supports the consideration that these tensors belong to the Al site of the M-Al-M groups. Within the original and the new models of the o-$Al_{13}Co_4$, the site symmetry of the Al atoms in the Co-Al-Co groups is $m..$, so that these Al atoms are sitting on the (100) mirror plane, causing the V_{ab} and V_{ac} elements to vanish by symmetry reasons. Within the two models of the $Al_{13}Fe_4$ phase, the site symmetry of the Al atom in the Fe-Al-Fe group is m, so that this Al atom is sitting on the (010) mirror plane, causing the V_{a^*b} and V_{bc} elements again to vanish by symmetry. The Al and the M site symmetries of the M-Al-M atoms for all four structural models are collected in Table II. The M sites do not exhibit any symmetry.

1. Point-charge calculation of the EFG for the M-Al-M charges

In the first step, we perform a point-charge calculation of the EFG tensor elements by considering the electric charges on the M-Al-M group only. The EFG at the Al site is determined by the two M ionic charges and by the electronic density on the M-Al covalent bonds. We simplify the problem by assuming that the charges on each side of the Al atom of the M-Al-M group can be replaced by a point charge e at a distance r from the Al atom. The coordinate system is chosen such that the M-Al-M planar group lies in the (x,z) plane with the Al atom at the origin and the position vector of a given charge forms an angle φ with the z axis and an angle $\beta/2$ with the x axis (Fig. 7), where $2\varphi+\beta=180°$. The EFG tensor elements V_{ij} are calculated from the formula

$$V_{ij}=\sum_k \frac{e_k(3x_i^k x_j^k - r_k^2\delta_{ij})}{r_k^5}, \tag{5}$$

where $x_i,x_j=x,y,z$ and $k=1,2$. We obtain

$$V_{xx}=\frac{2e}{r^3}(3\sin^2\varphi-1), \tag{6a}$$

$$V_{yy}=-\frac{2e}{r^3}, \tag{6b}$$

$$V_{zz}=\frac{2e}{r^3}(3\cos^2\varphi-1) \tag{6c}$$

and $V_{xy}=V_{xz}=V_{yz}=0$. For small angles φ (as it is the case for all the $Al_{13}M_4$ phases), the diagonal elements appear in the order $|V_{xx}|<|V_{yy}|<|V_{zz}|$ so that the asymmetry parameter can readily be computed from $\eta_w=(V_{xx}-V_{yy})/V_{zz}=3\sin^2\varphi/(3\cos^2\varphi-1)$ (where the subscript w denotes the Würstchen). The angles φ and β are slightly different for

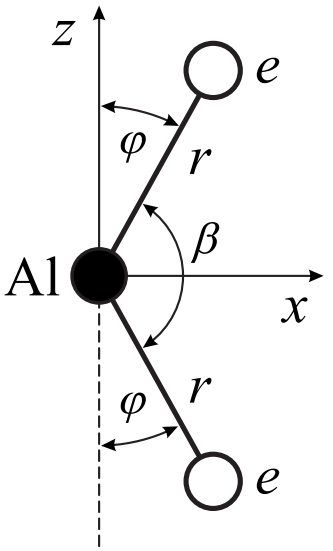

FIG. 7. Schematic representation of the M-Al-M group and the coordinate system for the point-charge calculation of the EFG tensor via Eqs. (5) and (6).

different structural models of the o-$Al_{13}Co_4$ and $Al_{13}Fe_4$ phases and are collected in Table III together with the corresponding η_w values. We observe that for all four models, these values are in the range $\eta_w \in [0.001,0.016]$, which is a factor about 10 smaller than the experimental values $\eta \in [0.07,0.11]$. This shows that the charges on the M-Al-M group alone are not enough to reproduce the EFG at the Al site. Instead, the distribution of the charges around the central Al atom is less axially symmetric, indicating that the charges of the Al cage atoms around the M-Al-M group should also be taken into account.

2. EFG calculation for the M-Al-M and the cage-atom charges

In the second step, we repeated the point-charge calculation of the EFG, this time by considering the charges of both the M-Al-M group and the surrounding cage atoms. The calculation was performed for the new o-$Al_{13}Co_4$ model, for which the structural detail of the Al cage with its Co-Al-Co guest is shown in Figs. 6(b) and 6(c), and for the refined $Al_{13}Fe_4$ model. For the computation of the asymmetry parameter η, the charges at all considered lattice sites (the M and the cage-atom positions) were taken equal. For the first of the two different Co-Al-Co groups in the unit cell of the new o-$Al_{13}Co_4$ model (the one with $\beta=174.66°$), the theoretical asymmetry parameter amounts $\eta_{c+w}=0.089$ (with the subscript $c+w$ denoting "cage plus Würstchen"), which is fairly close to the experimental value $\eta=0.07$. In contrast, by considering the cage atoms only, the asymmetry parameter amounts $\eta_c=0.29$ (with c denoting cage) that is much larger than the experimental η value. This confirms that the distribution of the cage-atom charges around the M-Al-M group is relatively far from being axially symmetric and demonstrates that both the M charges and the charges of the cage atoms contribute significantly to the EFG at the Al site of the M-Al-M group. This is in favor of the predominant ionic bonding between the M-Al-M group atoms and the surround-

TABLE III. Comparison of the experimental and theoretical values of the EFG-tensor asymmetry parameter η. β denotes the *M*-Al-*M* angle within a given structural model and φ is defined in Fig. 7. The theoretical asymmetry parameter η_w is calculated by considering the charges of the *M*-Al-*M* group only; η_c is the asymmetry parameter for the cage-atom charges only, whereas η_{c+w} is obtained by taking into account both the *M*-Al-*M* and the cage-atom charges.

Model	β (deg)	φ (deg)	Experiment	Theory		
			η	η_{c+w}	η_w	η_c
o-$Al_{13}Co_4$ [new (Ref. 12)]	175.14	2.43	0.07	0.062	0.003	0.229
	174.66	2.67	0.07	0.089	0.003	0.290
o-$Al_{13}Co_4$ [original (Ref. 3)]	170.46	4.77	0.07		0.011	
	168.30	5.85	0.07		0.016	
$Al_{13}Fe_4$ [refined (Ref. 17)]	177.18		0.11	0.056	0.001	0.213
$Al_{13}Fe_4$ [original (Ref. 4)]	176.87		0.11		0.001	

ing cage atoms. A very similar result is obtained also for the second Co-Al-Co group of the o-$Al_{13}Co_4$ unit cell, the one with β=175.14°. By taking into account both the *M* and the cage atoms, the theoretical asymmetry parameter amounts η_{c+w}=0.062, which is very close to the experimental value η=0.07. The asymmetry parameter of the cage atoms only is again much larger, η_c=0.229. The above theoretical η_{c+w} and η_c values are also collected in Table III.

The situation for the $Al_{13}Fe_4$ is similar (Table III). By taking into account both the Fe-Al-Fe group atoms and the cage atoms, the theoretical asymmetry parameter amounts η_{c+w}=0.056, which compares reasonably to the experimental value η=0.11. The asymmetry parameter due to the cage atoms only is again larger, η_c=0.21.

Here it is worth emphasizing that the employed point-charge model for the EFG calculation is a good approximation for the ionically bonded atoms of the cage, whereas it should be taken with reserve for the covalently bonded atoms within the *M*-Al-*M* groups, where an *ab initio* quantum chemical calculation of the asymmetry parameter is necessary to obtain a more reliable value of η_w (and consequently η_{c+w}). Our point-charge calculation should thus be considered as qualitative only (this also follows from the fact that all charges were taken equal in the calculation).

It is also worth noting that the experimental magnetic-shielding tensor asymmetry parameter ε values at the position of the Al atom in the *M*-Al-*M* group are reasonably close to the corresponding experimental EFG asymmetry parameter η values for all the investigated $Al_{13}M_4$ compounds (Table I). Since the symmetry of any local tensorial quantity is determined by the local site symmetry, the similar ε and η values are not surprising.

V. CONCLUSIONS

The crystallographic structures of the *d*-QCs and their periodic approximants are traditionally described as a periodic stacking of atomic planes. In order to see whether this pseudo-2D description is justified also from the chemical bonding scheme, or the compounds are true 3D solids, we performed a ^{27}Al NMR spectroscopic study of single crystals of the $Al_{13}M_4$ family of four-layer decagonal approximants, including the orthorhombic o-$Al_{13}Co_4$, the monoclinic $Al_{13}Fe_4$, its ternary derivative $Al_{13}(Fe,Ni)_4$, and the monoclinic $Al_{13}Ru_4$. By determining the EFG- and the magnetic-shielding tensors at the Al site of the *M*-Al-*M* groups, we showed that all these phases contain the structural detail of a nearly linear *M*-Al-*M* atomic group trapped inside an elongated cage, resembling the 3D cage-compound structure of the intermetallic clathrates. The asymmetry parameter of the EFG tensor at the Al site of the *M*-Al-*M* groups was estimated theoretically by a point-charge calculation, taking into account the charges of both the *M*-Al-*M* group and the surrounding cage atoms. The results support predominant ionic bonding of the *M*-Al-*M* group to the surrounding cage atoms and the existence of a 3D chemical bonding framework within the $Al_{13}M_4$ structures, reported previously for the o-$Al_{13}Co_4$ phase by the ELI analysis.[11,12] In contrast, the charges of the *M*-Al-*M* group or the cage atoms alone could not reproduce the experimental value of the asymmetry parameter. From the structural and the physical-property points of view, the $Al_{13}M_4$ decagonal approximants are true 3D solids. Their traditional description in terms of 2D atomic layers stacked along the pseudotenfold direction is a convenient geometrical approach to describe their complex structures but is not appropriate for the description of their physical properties, which should be analyzed by taking into account the full 3D nature of the chemical bonding framework. The above conclusions are drawn on the basis of experiments performed on the $Al_{13}M_4$ decagonal approximant phases that are translationally periodic in all three crystallographic directions. Due to the structural similarity of the approximants to the *d*-QCs, the same conclusions can be extrapolated to the *d*-QCs so that their physical properties should also be considered as those of a true 3D solid.

ACKNOWLEDGMENTS

This work was done within the Sixth Framework EU Network of Excellence "Complex Metallic Alloys" (Contract No. NMP3-CT-2005-500140). Slovenian authors acknowledge support from the Centre of Excellence EN→FIST, Dunajska 156, SI-1000 Ljubljana, Slovenia.

[1] For a review see, e.g., A. I. Goldman and K. F. Kelton, Rev. Mod. Phys. **65**, 213 (1993).
[2] B. Zhang, V. Gramlich, and W. Steurer, Z. Kristallogr. **210**, 498 (1995).
[3] J. Grin, U. Burkhardt, M. Ellner, and K. Peters, J. Alloys Compd. **206**, 243 (1994).
[4] J. Grin, U. Burkhardt, M. Ellner, and K. Peters, Z. Kristallogr. **209**, 479 (1994).
[5] L.-E. Edshammar, Acta Chem. Scand. **19**, 2124 (1965).
[6] Z. A. Chaudhury and C. Suranarayama, J. Less-Common Met. **91**, 181 (1983).
[7] L.-E. Edshammar, Acta Chem. Scand. **18**, 2294 (1964).
[8] D. W. Deng, Z. M. Mo, and K. H. Kuo, J. Phys.: Condens. Matter **16**, 2283 (2004).
[9] M. A. Taylor, Acta Crystallogr. **14**, 84 (1961).
[10] K. Hiraga, M. Kaneko, Y. Matsuo, and S. Hashimoto, Philos. Mag. B **67**, 193 (1993).
[11] M. Kohout, H. Borrmann, U. Burkhardt, R. Cardoso-Gil, F. Haarmann, P. Jeglič, A. Leithe-Jasper, T. Mori, Yu. Prots, W. Schnelle, M. Schmidt, O. Sichevich, I. Veremchuk, F. R. Wagner, and Yu. Grin, Max-Planck-Institut für Chemische Physik fester Stoffe, Scientific Report No. 2006–2008, 2009 (unpublished).
[12] Yu. Grin, B. Bauer, U. Burkhardt, R. Cardoso-Gil, J. Dolinšek, M. Feuerbacher, P. Gille, F. Haarmann, M. Heggen, P. Jeglič, M. Müller, S. Paschen, W. Schnelle, and S. Vrtnik, *EUROMAT 2007: European Congress on Advanced Materials and Processes*, Book of Abstracts (Nürnberg, Germany, 2007), p. 30.
[13] P. Jeglič, M. Heggen, M. Feuerbacher, B. Bauer, P. Gille, and F. Haarmann, J. Alloys Compd. **480**, 141 (2009).
[14] P. Gille and B. Bauer, Cryst. Res. Technol. **43**, 1161 (2008).
[15] J. Dolinšek, M. Komelj, P. Jeglič, S. Vrtnik, D. Stanić, P. Popčević, J. Ivkov, A. Smontara, Z. Jagličić, P. Gille, and Yu. Grin, Phys. Rev. B **79**, 184201 (2009).
[16] L. Zhang, Y. Du, H. Xu, C. Tang, H. Chen, and W. Zhang, J. Alloys Compd. **454**, 129 (2008).
[17] P. Popčević, A. Smontara, J. Ivkov, M. Wencka, M. Komelj, P. Jeglič, S. Vrtnik, M. Bobnar, Z. Jagličić, B. Bauer, P. Gille, H. Borrmann, U. Burkhardt, Yu. Grin, and J. Dolinšek, Phys. Rev. B **81**, 184203 (2010).
[18] See, e.g., J. Winter, *Magnetic Resonance in Metals* (Clarendon Press, Oxford, 1971), Chaps. II, IV, and V.
[19] See, e.g., M. Mehring, in *High Resolution NMR Spectroscopy in Solids*, NMR—Basic Principles and Progress Vol. 11, edited by P. Diehl, E. Fluck, and R. Kosfeld (Springer, Berlin, New York, 1976), p. 7.